





Investigation on Crack Control and Crack Pattern Analysis of Self-compacting Concrete Exposed to Standard Fire Exposure



Mervin Ealiyas Mathews , N. Anand , A. Diana Andrushia ,
and Tattukolla Kiran 

Abstract Development of thermal cracks is inevitable in concrete structures under extreme fire conditions. Intense heat flux on the exposed surface and the thermal incompatibility between the mortar and aggregate phase results in micro-cracks. The geometrical properties of cracks such as width, length, density and pattern are to be quantified accurately to adopt suitable control methods. This study aims to analyse the crack pattern and crack control measures on Self-Compacting Concrete (SCC) exposed to standard fire temperature. SCC mixes were developed to achieve a strength of 30MPa using Fly Ash (FA), Ground Granulated Blast Furnace Slag (GGBFS) and Expanded Perlite Aggregate (EPA). The rheological behaviour of the developed mixes was confirmed as per European Federation of National Associations Representing for Concrete (EFNARC 2005) guidelines. After the curing process, specimens were exposed to elevated temperatures for different durations (30, 60, 90, and 120 min) following the International Organization for Standardization ISO 834 standard fire curve. A mortar combination of Cement-Perlite Plaster (CPP) was considered as the sacrificial layer (protection layer) over the concrete surface to understand the efficiency of perlite in controlling the crack growth. GGBFS-SCC specimens exhibited severe surface cracking than FA-SCC specimens. The protected (CPP) specimens showed better resistance on mitigating the surface cracks even at 120 min of heating. Attempts have been made to quantify the cracks on the concrete surface with the help of Image-Processing Tool (IPT). Scanning Electron Microscopy (SEM) analyses have been carried out to analyse the micro-cracks in the fire-damaged concrete.

Keywords Self-compacting concrete · Elevated temperature · Thermal cracks · Image processing · EFNARC

M. E. Mathews (✉) · N. Anand · A. D. Andrushia · T. Kiran
Karunya Institute of Technology and Sciences, Coimbatore, India

© RILEM 2021

F. Kanavaris et al. (eds.), *International RILEM Conference on Early-Age and Long-Term Cracking in RC Structures*, RILEM Bookseries 31,
https://doi.org/10.1007/978-3-030-72921-9_11

127

1 Introduction

Concrete has many versatile characteristics and advantages in contrast to other construction materials. Some of them are compressive strength, inherent fire resistance, cost-effectiveness in implementing the construction projects [1]. However, the cracks in concrete persist in its plastic and hardened form due to various causes, as shown in Fig. 1. The crack formation and propagation adversely affect the durability of concrete [2].

According to the American Concrete Institute, the term durability is stated as the ability to remain serviceable, retain quality and stability even after exposed to critical environmental conditions or accidental events [3]. The intensity of surface crack generation and propagation on hardened concrete due to unexpected fire is larger than the cracks formed by other durability problems. As the concrete becomes more brittle after the exposure of fire, these cracks gain more importance in reducing the service life of concrete structures [4]. The effect of fire-induced damages ultimately affects the durability of concrete structures. The intense irregular formation of surface cracks causes a discontinuity in the particle phase and reduce the local stiffness [5]. Proper, timely assessment and preventive measures to reduce the crack induced damages that will be useful to avoid structural failure [6].

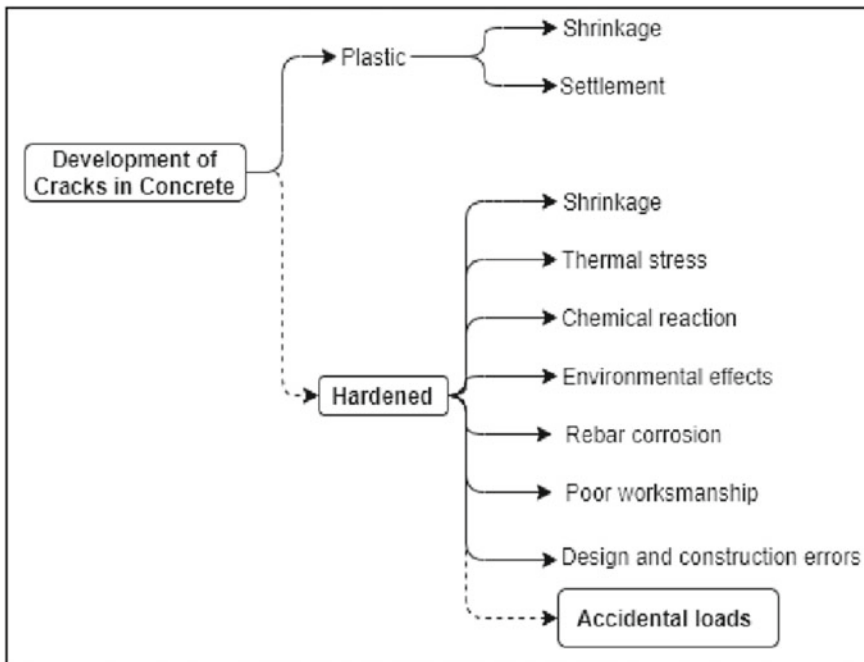


Fig. 1 Development of cracks in concrete as per ACI

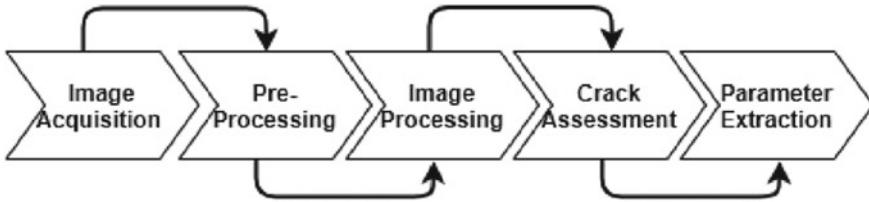


Fig. 2 Structural flow of crack detection and analysis based on IPT

Destructive Testing (DT) and Non-Destructive Testing (NDT) are the methods for crack detection and assessment with the help of human visual observations and inspecting tools thereby the surface deformities can be assessed and evaluated [7]. The reduction in the load-carrying capacity and durability level of the concrete structure can be predicted by evaluating the crack properties such as type, length, width, and density of surface cracks [8]. The human inspective methods of surface crack evaluation can be done quickly and instantly, but the concerns about accuracy and localized evaluation restriction exist, also its objective-based deterioration analysis is complicated [9]. Automatic surface defect analysis is being developed with the help of various image processing tools (IPT) to overcome the drawbacks of manual inspection [10]. This will enhance the accuracy of damage assessment, allows objective deterioration evaluation and the process can be executed with high efficiency. Infrared (IR), ultrasonic, laser, thermal and radiographic methods are other assessment adopted for crack defects identification [9].

The crack detection and analysis based on IPT is having great interest among researchers because of its simplicity and reliability [11, 12]. Algorithmic, morphological, percolation and practical based methods are the four approaches generally adopted in IPT procedures [13]. The typical image processing difficulties are noise, shades, blemish and sharpness, which are expected while extracting the results. Figure 2 explicit the structural flow of crack detection and analysis based on IPT.

The main objective of the present work is to assess and analyse the effect of temperature on the crack intensifying nature of SCC specimens developed with FA, GGBFS and EPA. Manual inspection and observations were made using inspecting tools, and the mean width of the visually largest crack is noted. IPT based crack detection and quantification were used to analyse the damage level of the fire exposed concrete. Scanning Electron Microscopy (SEM) based microstructure analysis was carried out to understand the particle phase discontinuities in the fire affected concrete. The outcome of the results was used to develop a crack control mortar combination of CPP over the concrete surface to understand the efficiency of perlite in controlling the crack growth.

2 Experimental Program

The experimental investigation focused on analysing the effect of temperature on the formation of surface cracks on the SCC specimen developed with FA and GGBFS. To understand the effectiveness of perlite in regulating the crack growth, a mortar combination of CPP was wrapped over the concrete surface. The maximum temperature simulates the heat effect of a real fire varied from Room Temperature (RT) to 1029 °C following ISO 834 fire rating curve. Siliceous aggregates are used for the development of concrete mixes.

2.1 Mix Proportion

Four different SCC mixes were developed, and the mix proportioning is stated in Table 1. Ordinary Portland Cement (OPC) of 53-grade was used for the investigation. The slump flow test assessed the consistency and workability of fresh SCC. The flow spread diameter values were measured between 660 and 680 mm, and it satisfies the permissible limit stipulations of EFNARC 2005 [14].

Mineral Admixtures

Class-F FA and GGBFS are the industrial by-products, used as a replacement material for cement in the development of SCC mix. The chemical and physical properties of materials are given in Table 2.

Aggregates

Crushed granite stones of maximum 12 mm size and Manufactured Sand (M-Sand) with a maximum particle size of 4.75 mm were used as coarse and fine aggregate respectively for Mix 1 and Mix 3. Mix 2 and Mix 4 consist of 2.5% fine aggregate is replaced with EPA content to understand the fire resistance capability of perlite in the SCC core structure. The optimum level of EPA is achieved as 2.5% by different trial on fresh concrete. This mix satisfied the strength requirement of hardened concrete at elevated temperature. The properties of EPA is given in Table 2.

Table 1 Mix proportions of SCC

Description	Cement/Mineral admixtures	Aggregates (coarse/fine; EPA)	Water	Chemical admixtures (SP/VMA)
	(kg/m ³)			
Mix 1	320/144(FA)	804/963	218	0.80/0.10
Mix 2	320/144(FA)	804/939; 24 (EPA)	218	0.90/0.15
Mix 3	320/144(GGBFS)	804/963	218	0.90/0.15
Mix 4	320/144(GGBFS)	804/939; 24 (EPA)	218	1.0/0.20

Table 2 Characteristics of the materials

Material	Chemical composition (%)						Physical property	
	CaO	SiO ₂	Al ₂ O ₃	Fe ₂ O ₃	MgO	K ₂ O	Specific gravity	Fineness (m ² /kg)
OPC	61.33	18.78	8.75	3.40	2.25	2.20	3.15	335
FA	2.25	58.50	28.25	3.45	0.30	1.26	2.60	306
GGBFS	37.34	37.73	14.42	1.11	8.71	–	2.90	441
EPA	0.6–2.40	72–76	11–16	0.6–1.40	–	2–5	0.055–0.30	–

Water

Potable water is used throughout the experimental investigation for developing, casting and curing.

2.2 Details of Test Specimens

Test specimens with a diameter of 150 mm and a height of 63.50 mm are used for the investigation. It is decided to conduct a surface crack assessment on cylindrically shaped samples. As the cylindrical shape undergoes comparatively more uniform heating for varying heating cycles, it is preferable. Also, the formation of surface cracks on the exposed face will be ideally distributed across the cross-section, but in case of square or rectangular specimens, the crack distribution is more seen in corner regions due to the heat flux causing high-stress concentration in that region. The heating procedure is carried out on two different specimen conditions. The unprotected specimens are taken for heating after the curing period without plastering. The protected (with CPP layer) specimens were cast with plaster of OPC and EPA mortar (1:4). Both the unprotected and protected specimens were dried for 24 h before taking it for heating in the furnace. The view of the test specimens and heating of specimen in the furnace is shown in Fig. 3.

2.3 Test Methodology and Heating Procedures

The test methodology is as follows:

- Preparation of test specimens (FA; FA/ CPP; FA/EPA; FA/EPA/ CPP; GGBFS; GGBFS/ CPP; GGBFS/EPA and GGBFS/EPA/ CPP) [Details of test specimens id are mentioned in Table 3].
- Curing process for 28 days.
- Specimens kept for drying in laboratory conditions at RT (for 24 h).
- Selected batch of specimens are wrapped with CPP layer.

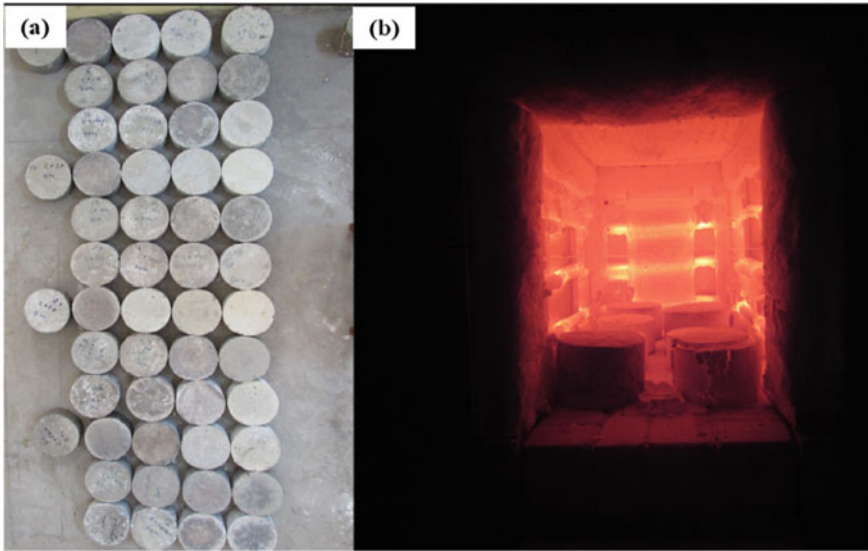


Fig. 3 a View of the test specimens. b Heat test of specimen in computerised electrical furnace

- Heating of specimens following ISO 834 fire rating curve (for 821 °C at 30, 925 °C at 60, 986 °C at 90, and 1029 °C at 120 min) [15].
- Crack detection and analysis.

The content of moisture inside the specimen was measured by taking the difference between the actual weight and the weight of the specimens after heat exposure, and it was noted that moisture loss was varying between 1.5 and 6.5%.

The importance of simulating the real effect of fire was of great concern in this study. The rate of heating and duration of the heating pattern was followed similar to the standard fire curve (ISO 834) with the help of an integrated microprocessor-based control panel in the electric furnace. The duration considered for the study is 30, 60, 90, and 120 min. Once the target temperature is reached, the furnace turns off automatically. After that, the specimens were taken out, and the necessary natural cooling is provided.

3 Test Results and Discussions

3.1 *Effect of Elevated Temperature and Mineral Admixtures on Crack Development*

The temperature and duration of the fire exposure have a significant effect on the surface crack formation and its growth. Figure 4 shows the captured surface images

Table 3 Measured crack width of SCC specimens at different durations of heating

Specimen id	Crack width (mm)				Remarks
	W_{min}	W_{max}	W_{avg}	$W_{std.dev}$	
FA/_CPP 0M	0.00	0.00	0.00	0.00	FA-SCC Specimens with CPP layer
FA/_CPP 30M	0.00	0.00	0.00	0.00	
FA/_CPP 60M	0.02	0.04	0.03	0.01	
FA/_CPP 90M	0.04	0.06	0.05	0.01	
FA/_CPP 120M	0.18	0.20	0.19	0.07	
FA/EPA 0M	0.00	0.00	0.00	0.00	FA-SCC Specimens with EPA as filler material
FA/EPA 30M	0.02	0.04	0.03	0.01	
FA/EPA 60M	0.09	0.12	0.11	0.04	
FA/EPA 90M	0.16	0.20	0.18	0.05	
FA/EPA 120M	0.26	0.28	0.27	0.06	
FA/EPA/ CPP 0M	0.00	0.00	0.00	0.00	FA-SCC Specimens with EPA as filler and CPP layer
FA/EPA/ CPP 30M	0.00	0.00	0.00	0.00	
FA/EPA/ CPP 60M	0.01	0.02	0.02	0.01	
FA/EPA/ CPP 90M	0.07	0.08	0.08	0.03	
FA/EPA/ CPP 120M	0.09	0.12	0.11	0.05	
GGBFS/ CPP 0M	0.00	0.00	0.00	0.00	GGBFS-SCC Specimens with CPP layer
GGBFS/ CPP 30M	0.01	0.02	0.02	0.01	
GGBFS/ CPP 60M	0.02	0.04	0.03	0.01	
GGBFS/ CPP 90M	0.13	0.16	0.15	0.04	
GGBFS/ CPP 120M	0.24	0.26	0.25	0.06	
GGBFS/EPA 0M	0.00	0.00	0.00	0.00	GGBFS-SCC Specimens with EPA as filler material
GGBFS/EPA 30M	0.11	0.12	0.12	0.05	
GGBFS/EPA 60M	0.20	0.22	0.21	0.08	
GGBFS/EPA 90M	0.29	0.30	0.29	0.10	
GGBFS/EPA 120M	0.31	0.36	0.33	0.12	
GGBFS/EPA/ CPP 0M	0.00	0.00	0.00	0.00	GGBFS-SCC Specimens with EPA as filler and CPP layer
GGBFS/EPA/ CPP 30M	0.00	0.00	0.00	0.00	
GGBFS/EPA/ CPP 60M	0.01	0.02	0.02	0.01	
GGBFS/EPA/ CPP 90M	0.15	0.18	0.17	0.05	
GGBFS/EPA/ CPP 120M	0.18	0.20	0.19	0.07	

and the thermal crack width of different unheated and heated SCC specimens. It was noted that as the rate and duration of heat exposure increases, the crack width also increases significantly. The magnified visuals of measuring crack width are enclosed within the actual view of the surface images. The crack width is measured using the Elcometer. The density of the surface crack increased drastically as the duration of heating increases from 30 to 120 min.

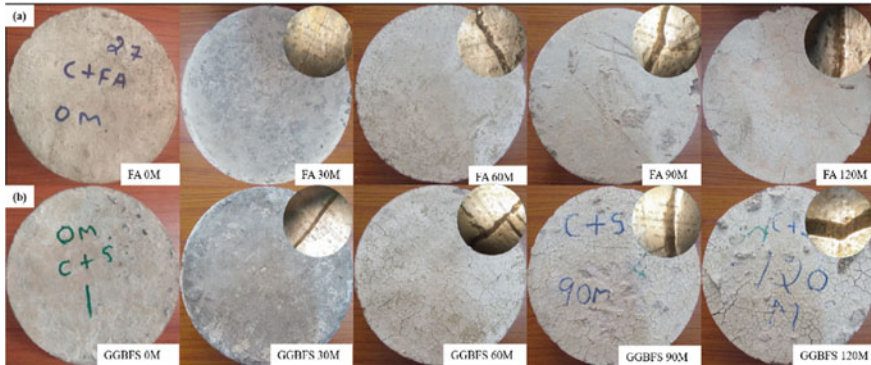


Fig. 4 View of thermal crack width (Unheated and heated SCC specimens). **a** FA-SCC specimens. **b** GGBFS-SCC specimens

Figure 5 shows the plot showing the duration of heating and the average crack width of SCC specimens developed with FA and GGBFS. The data is formulated by recording several numbers of crack width measured with mean values. It is observed from the plot that GGBFS-SCC specimens has comparatively larger surface thermal cracks compared to FA-SCC specimens. The 30 min heated FA-SCC specimens (FA 30M) had 0.02 mm of average crack width ($W_{avg.}$), but in case of GGBFS-SCC specimens (GGBFS 30M) heated for 30 min, the $W_{avg.}$ were found to be 0.10 mm.

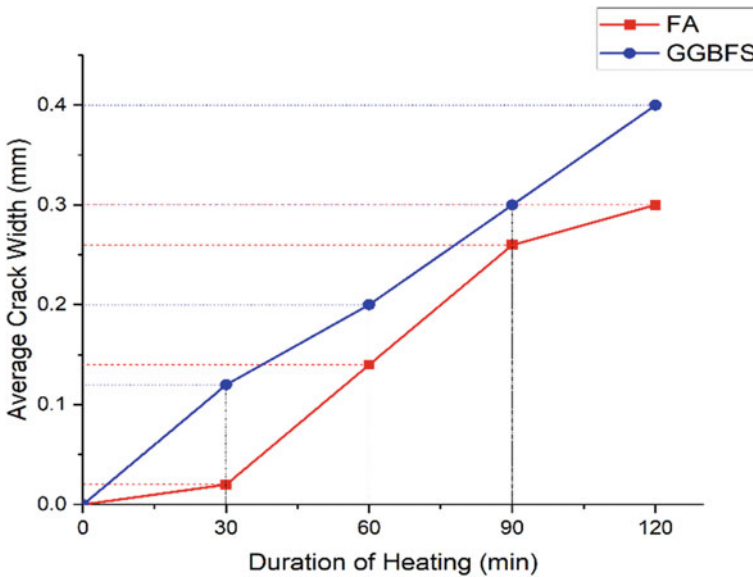


Fig. 5 Average crack width of FA-SCC and GGBFS-SCC specimens

The $W_{avg.}$ values observed for 120 min heated specimens of FA (FA 120M), and GGBFS (GGBFS 120M) are 0.29 mm and 0.39 mm respectively.

3.2 Effect of CPP Technique on Surface Crack Control of SCC

In the previous phase of the study, an analysis carried out regarding the effect of elevated temperature and the variation in the crack intensity of SCC specimens with different admixtures. Subsequently, in the second phase of the investigation, authors have attempted to develop a crack control method to reduce the effect of heat directly falling on the SCC surface by incorporating the EPA as a protective coating material. The study has been carried out in three different ways such that by adding EPA at an optimum level (2.5% of fine aggregate content) as internal filler material along with the powder (binder) content, as a mortar combination of Cement-Perlite Plaster (CPP) was considered as the sacrificial layer (protection layer) over the concrete surface and at last a combination of the EPA as filler and CPP layer.

Table 3 illustrates the summary of results recorded in terms of minimum, maximum, average and standard deviation of crack width measured using Elcometer on the surface of FA-SCC specimens and GGBFS-SCC specimens exposed to elevated temperature. The significant surface crack formation was not observed up to 30 min of heating. Notable surface rupture was noticed between 30 and 120 min of heating. It is noted that in the test specimens without protective CPP layer exposed to 120 min of heating has a significant effect on wider surface crack development. The protected specimens with CPP layer in both the FA and GGBFS-SCC specimens (i.e., FA/EPA/CPP, FA/CPP, GGBFS/EPA/CPP & GGBFS/CPP) were resistant to the expansion of crack even at 120 min. But as noted in the previous section, significant surface cracks were observed due to heat even at 60 min of heating for both the specimens FA and GGBFS, without EPA and CPP. This clearly shows the effectiveness of the protection technique using EPA mineral as a sacrificial material.

3.3 SEM Analysis

SEM analysis is carried out to understand the effect of damage incurred inside the SCC core due to elevated temperature exposure. As visual observations help identify the surface damage concerning thermal cracks, SEM analysis is helpful to understand the morphological changes that happened inside the SCC structure before and after heating. The cracks and voids increases, as the exposure duration increases for FA and GGBFS specimens. Also, the CPP layer had protected specimens from the severe effect of fire. Figure 6 shows the SEM images of 120 min heat-exposed specimens (a) FA-SCC specimens, (b) GGBFS-SCC specimens.

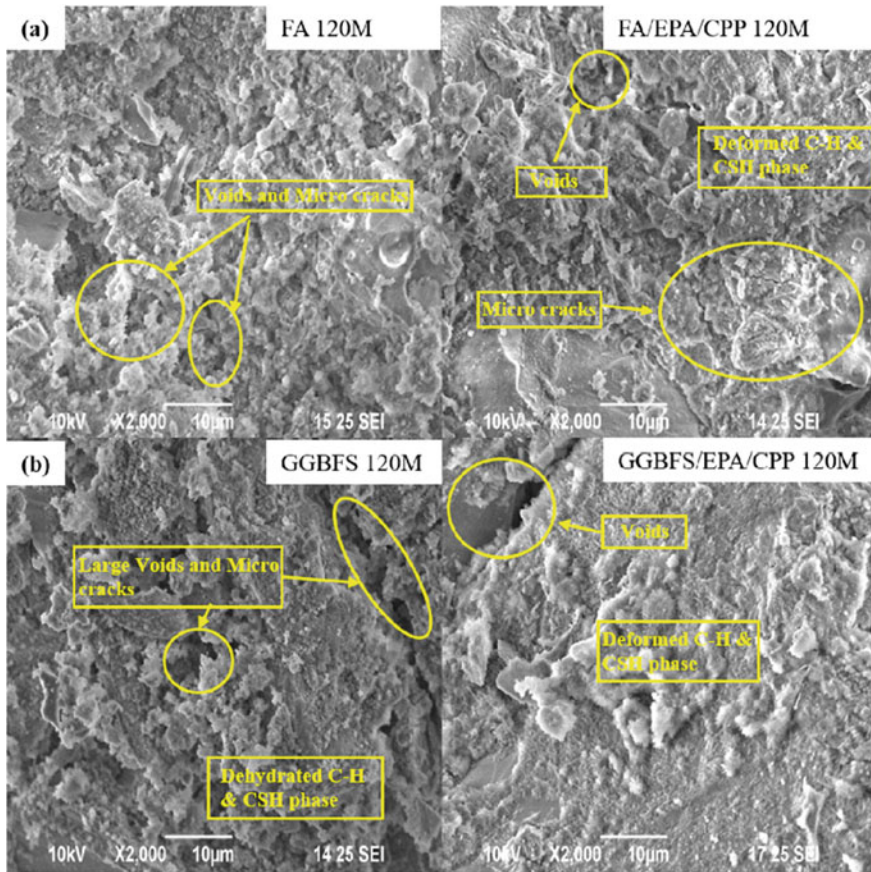


Fig. 6 SEM images of heat-exposed specimens. **a** FA-SCC specimens. **b** GGBFS-SCC specimens

3.4 IPT Analysis

The input images are collected from real-time experiments, i.e., FA and GGBFS based SCC exposed to 120 min duration. In both the cases, CPP and EP/ CPP type specimens are used for the analysis. The image collection setup consists of the Canon SX510 HS camera for taking a photograph with optical image stabilizer of intelligent IS for sharp photos. It has 30x optical zoom with 24 mm wide lens in a mini body. It has 60x Zoom Plus HS System with 12.1 Megapixel CMOS having DIGIC 4 facility and can produce quality capture even in low light. The image analysis experiment is performed with the help of MATLAB 2018 software.

The image-based damage analysis consists of two significant steps, namely damage detection and quantification. To identify the damages clearly, the input images are applied with the prerequisites process of background estimation and noise removal. The damage detection is done through the method specified in A DA

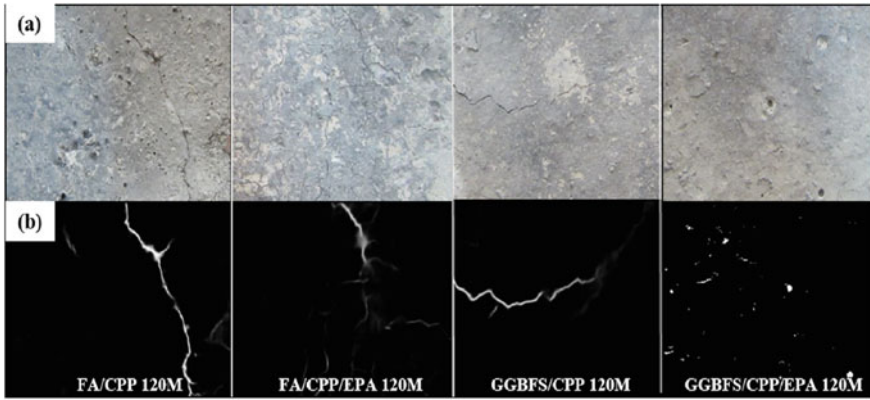


Fig. 7 Image analysis based damage detection of heat exposed FA and GGBFS SCC specimen. **a** Raw images. **b** Processed images

[16]. Initially, the input images are decomposed into higher and lower sub-bands. The uneven backgrounds are removed with the help of column filtering. Ripplet Coefficient Variance Parameter (RCVP) is leveraged to separate the crack pixel from the noisy pixels in the sub-bands. The directional properties of ripplet transform are used to identify the weak cracks. All the cracks are identified in the reconstructed images. Figure 7 shows the input images of FA and GGBFS based concretes and their corresponding damages.

The damage quantification is done after the crack detection process. The morphological information of cracks is used to quantify the cracks. The morphological operations such as closing, opening, pruning and thinning are used to determine the crack properties. Thinning process is used to perform skeletonization with respect to branch point processing [17]. The isolated pixels which are related to noises are removed by the cleaning process. Let $m(x, y)$ be the skeleton point index as given in Eq. (1), which regulates the displacement of the point in the detected cracks from the input image [18].

$$m(x, y) = \begin{cases} 1, & (x, y) \in \text{skeleton} \\ 0, & \text{otherwise} \end{cases} \quad (1)$$

The length of the cracks can be obtained from the skeleton points using the Eq. (2).

$$z_l = \int m(x, y) dz \quad (2)$$

where dz represents pixel level, finite crack length at the skeleton line. The particular distance between two adjacent points is calculated using the Eq. (3),

$$m((x_{i+1} - x_i)^2 + (y_{i+1} - y_i)^2)^{1/2} \quad (3)$$

Sebastien demonstrated the crack detector for inputs. Thus, the crack properties of crack length and crack width are obtained [19]. The damage quantification is calculated through the total crack length attribute. The input images are resized into 512×512 . The total crack length of FA-CPP and GGBFS-CPP based concretes are 143.23 and 872.3 pixels. It is evident from the analysis that, concrete with GGBFS exhibited significant damage in terms of thermal crack.

4 Conclusion

The main objective of this research was about to investigate the effective crack control measures that can be adopted on SCC specimens exposed to standard fire based on the analysis of crack pattern. The surface cracks developed due to the high-temperature exposure will lead to severe durability problems and thereby reduces the overall service life of the structure. Therefore, crack assessment and control are the control factors in the proper health monitoring of SCC structures.

Here, an extensive surface crack property has been carried out using conventional crack property surveying tool (Elcometer) and the IPT. The properties of ripplet transform were used in the IPT approach to assessing the fire induce crack parameters. Also, the SEM analysis was incorporated into the study to understand the internal deformation incurred due to high-temperature exposure. The outcome of the study clearly shows the effectiveness of perlite as a protective material in the form of internal filler as well as a mortar combination of CPP layer. The development of surface cracks generation and propagation has been significantly delayed on the protected SCC specimens compared to the unprotected. The novel method of assessing the heat-induced cracks and the crack control method suggested in work can be effectively implemented on the structures subjected to accidental fires.

References

1. Aboalarab, L.: The effect of crack opening size and repair methods on corrosion of steel reinforcement in concrete (2019)
2. 224, A.C., 224, A.C.: Causes, evaluation and repair of cracks in concrete structures, ACI 224.1R-93. Man. Concr. Pract. (1998)
3. ACI 201.2R-01: Guide to durable concrete reported by ACI Committee 201. ACI Comm. **201** (2008)
4. Mathews, M.E., Nandhagopal, M., Anand, N., Arulraj, G.P.: Versatility at its best: an integrated review on development of self-compacting concrete. *Int. J. Sci. Technol. Res.* **8**, 513–519 (2019)
5. Thanaraj, D.P., Anand, N., Prince Arulraj, G., Zalok, E.: Post-fire damage assessment and capacity based modeling of concrete exposed to elevated temperature. *Int. J. Damage Mech.* (2020). <https://doi.org/10.1177/1056789519881484>

6. Barris, C., Torres, L., Vilanova, I., Miàs, C., Llorens, M.: Experimental study on crack width and crack spacing for Glass-FRP reinforced concrete beams. *Eng. Struct.* (2017). <https://doi.org/10.1016/j.engstruct.2016.11.007>
7. Dhital, D., Lee, J.R.: A fully non-contact ultrasonic propagation imaging system for closed surface crack evaluation. *Exp. Mech.* (2012). <https://doi.org/10.1007/s11340-011-9567-z>
8. Shan, B., Zheng, S., Ou, J.: A stereovision-based crack width detection approach for concrete surface assessment. *KSCE J. Civ. Eng.* (2016). <https://doi.org/10.1007/s12205-015-0461-6>
9. Fujita, Y., Hamamoto, Y.: A robust automatic crack detection method from noisy concrete surfaces. *Mach. Vis. Appl.* (2011). <https://doi.org/10.1007/s00138-009-0244-5>
10. Mohan, A., Poobal, S.: Crack detection using image processing: a critical review and analysis. *Alexandria Eng. J.* (2018). <https://doi.org/10.1016/j.aej.2017.01.020>
11. Manjurul Islam, M.M., Kim, J.M.: Vision-based autonomous crack detection of concrete structures using a fully convolutional encoder–decoder network. *Sensors (Switzerland)* (2019). <https://doi.org/10.3390/s19194251>
12. Valença, J., Dias-da-Costa, D., Gonçalves, L., Júlio, E., Araújo, H.: Automatic concrete health monitoring: assessment and monitoring of concrete surfaces. *Struct. Infrastruct. Eng.* (2014). <https://doi.org/10.1080/15732479.2013.835326>
13. Wang, P., Huang, H.: Comparison analysis on present image-based crack detection methods in concrete structures. In: *Proceedings—2010 3rd International Congress on Image and Signal Processing, CISP* (2010). <https://doi.org/10.1109/CISP.2010.5647496>
14. EFNARC: The European guidelines for self-compacting concrete: specification, production and use (2005)
15. ISO 834-1: Fire-resistance tests—elements of building construction—part 1: general requirements. *ISO Stand* (1999)
16. Andrushia, A.D., Anand, N., Arulraj, G.P.: A novel approach for thermal crack detection and quantification in structural concrete using ripplelet transform. *Struct. Control Heal. Monit.* (2020). <https://doi.org/10.1002/stc.2621>
17. Arena, A., Delle Piane, C., Sarout, J.: A new computational approach to cracks quantification from 2D image analysis: application to micro-cracks description in rocks. *Comput. Geosci.* (2014). <https://doi.org/10.1016/j.cageo.2014.01.007>
18. Ji, A., Xue, X., Wang, Y., Luo, X., Xue, W.: An integrated approach to automatic pixel-level crack detection and quantification of asphalt pavement. *Autom. Constr.* (2020). <https://doi.org/10.1016/j.autcon.2020.103176>
19. Drouyer, S.: An “all terrain” crack detector obtained by deep learning on available databases. *Image Process. Line.* (2020). <https://doi.org/10.5201/ipol.2020.282>